ELSEVIER

Spectrochimica Acta Part B 63 (2008) 367–374

SPECTROCHIMICA ACTA PART B

www.elsevier.com/locate/sab

Laser induced breakdown spectroscopy on metallic alloys: Solving inhomogeneous optically thick plasmas

Cristian A. D'Angelo *, Diego M. Díaz Pace, Graciela Bertuccelli, Daniela Bertuccelli

Instituto de Física 'Arroyo Seco', Facultad de Ciencias Exactas, U.N.C.P.B.A., Pinto 399, B7000GHG Tandil, Argentina

Received 4 May 2007; accepted 24 October 2007
Available online 3 December 2007

Abstract

In this work, laser-induced breakdown spectroscopy (LIBS) has been applied to the characterization of a plasma generated on a ternary Co–Cr–Mo alloy commonly used on hip prosthesis in air at atmospheric pressure. A method to achieve analytical results without employing any reference sample was implemented within a two-region plasma picture of a hot dense core surrounded by a colder periphery, where both self-absorption and inhomogeneity effects were taken into account. High resolution spectra of three strong Co I–II lines from different regions of the plasma plume were recorded and the analysis was carried out by means of a least-squares calibration-free algorithm. In this approach, theoretical spectra were matched to the experimental line profiles. Thus, the plasma parameters (temperature, atom, ion and electron densities) and the line widths were obtained, demonstrating the feasibility of the method to characterize the physical state of a laser-induced plasma.

Keywords: Laser; Plasma; Analytic spectroscopy

1. Introduction

Laser-induced breakdown spectroscopy (LIBS) is a powerful analytical technique with a wide range of applications concerning both fundamental purposes and material analysis [1–4]. Currently, laser-induced plasmas (LIP) in air at atmospheric pressure are very useful for analysis of the elemental composition of solid samples such as metallic alloys, due to its inherent advantages of lack of any previous sample preparation and on-line measurement capability. In particular, Co–Cr–Mo alloys are currently employed in Medicine on prosthesis and orthopedic implants. Manufacturing of these bio-compatible alloys is very expensive and it should be characterized with minimum damage in order to study the influence of its composition on critical features such as fatigue and corrosion resistance [5].

Several works dealing with laser-induced plasmas for qualitative and quantitative analysis of metallic alloys can be found in the literature [6–10]. The analytical performance of the technique may be affected by self-absorption and spatial inhomogeneity [11–12]. In fact, due to the high density of atoms and ions present in laser-induced plasmas self-absorption of the spectral lines usually occurs within the plasma, which is said optically thick. Moreover, it is well-known that because LIP are spatially inhomogeneous, the plasma parameters have spatial distributions that evolve with time [13,14]. Therefore, the measured spectral lines have contributions due to the emission from regions with different values of the plasma parameters along the direction of observation. In an inhomogeneous optically thick LIP the strongly absorbed lines result self-reversed.

In order to quantify the analysis, the conventional method is using calibration curves constructed with reference samples [15]. Due to self-absorption, the intensity of the lines saturate and the calibration curves bend for concentrations higher than a critical value depending on its spectroscopic features and the experiment. The sensitivity of the curve decreases and the measured line intensity is not proportional to the element concentration in the sample. The plasma temperature is calculated by the Boltzmann plot method using the integrated line intensities of the measured spectral lines, rejecting those transitions showing self-absorption. Some researches asserted that self-absorption effects can be

* Corresponding author. Postal address: Pinto 399, B7000GHG Tandil, Argentina. Tel.: +54 2293 439661; fax: +54 2293 439669.
E-mail addresses: cdangelo@exa.unicen.edu.ar (C.A. D'Angelo), ddiaz@exa.unicen.edu.ar (D.M. Díaz Pace), gbertucc@exa.unicen.edu.ar (G. Bertuccelli), dbertucc@exa.unicen.edu.ar (D. Bertuccelli).

0584-8547/$ - see front matter © 2007 Elsevier B.V. All rights reserved.
doi:10.1016/j.sab.2007.10.049

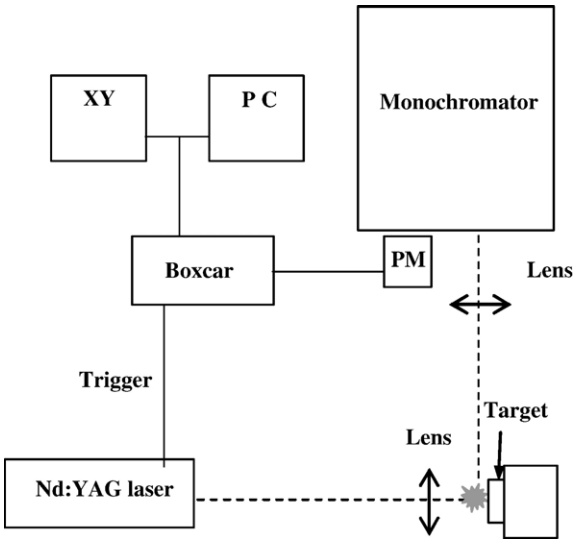

Fig. 1. Experimental set-up used in the present work for LIBS experiment.

reduced generating the plasma with relatively high laser energy under a low pressure atmosphere of an inert gas [9–11] or selecting for the analysis atomic transitions from high excited levels [6]. However, depending on the experimental situation, those lines are usually weak and seldom detected.

In many important applications dealing with unique samples (museum pieces and archaeological findings), unknown or complex matrix samples (rocks from planetary exploration missions), or expensive manufacturing process (medical prosthesis) reference samples are not available and an alternative LIBS analysis is needed, requiring rapid, in-situ and nondestructive measurements. Recently, several calibration-free analytical methods have been reported based on plasma physics to characterize the plasma state, overcoming

Table 1
Experimental set-up and settings used in this work

Laser	Pulsed Q-Switched Nd:YAG Big Sky
Pulse width	7–8 ns
Energy	10–50 mJ
Wavelength	1064 nm
Repetition Rate	1–20 Hz
Optics	
Focusing sample lens	Antireflection coated quartz, 10 cm focal length
Focusing monochromator lens	Quartz, 20 cm focal length
Detection system	
Monochromator	Jovin Yvon, Czerny Turner configuration
Resolution	300000 in double pass
Dispersion	0.13 nm/mm (at 300 nm)
Grating	Holografic ruled 2400 groves/mm
Slit widths (entrance/exit)	40/40 mm
Photomultiplier	Hamamatsu IP28
Spectral response range	200–600 nm
Signal processing	
Gated integrator and boxcar averager	Stanford Research Systems
Delay time	1500 ns
Gate width	30 ns
Trigger	External, from laser Q-switch output

Table 2
Spectral lines of Co employed for LIBS analysis

Element	Wavelength (nm)	A_{ji} (s^{-1})	g_j	g_i	E_j (eV)	E_i (eV)
Co I	340.51	1.0E8	10	10	4.07	0.43
	356.94	1.5E8	8	8	4.39	0.92
Co II	362.12	2.6E6	9	7	5.63	2.20

matrix effects. The basic assumptions are: (i) The plasma composition is representative of that of the target previous to the ablation (stoichiometric ablation); and (ii) The plasma is in local thermal equilibrium (LTE) in the time and spatial conditions of measurement. For instance, Hermann et al. [16] have shown that more precise evaluation of the plasma parameters can be achieved when self-absorption of the lines and plasma inhomogeneity are considered by using a model of a plasma divided in two uniform zones having different densities and/or temperatures. Preliminary estimations of kT_e and n_e were obtained from the Boltzmann plot method and the Stark broadening effect, respectively, of the emission lines from a LIP generated in a Ti target in a low pressure nitrogen atmosphere. More accurate values of the plasma parameters were then determined computing the spectral line profiles of three Ti II transitions under various conditions in order to reproduce the measurements. Bulajic et al. [17] developed a procedure for correcting self-absorption in the analysis of materials by LIBS without calibrations standards using a recursive algorithm. In their approach, plasma homogeneity and knowledge of all the species present in the plume are assumed. The method was tested with three ternary alloys of known composition, improving the precision and the accuracy. In the work of Aguilera et al. [18] the effects of self-absorption and plasma inhomogeneity on the curves of growth (COGs) of five Fe lines recorded from a LIP generated with Fe–Ni alloys with different concentrations have been studied by means of a fitting program based on a two-region plasma framework for the initial times of the plasma evolution and on a single-region model for the later times where the LIP has expanded and cooled. The plasma parameters were determined by comparison of the theoretical and experimental curves. This set of parameters was

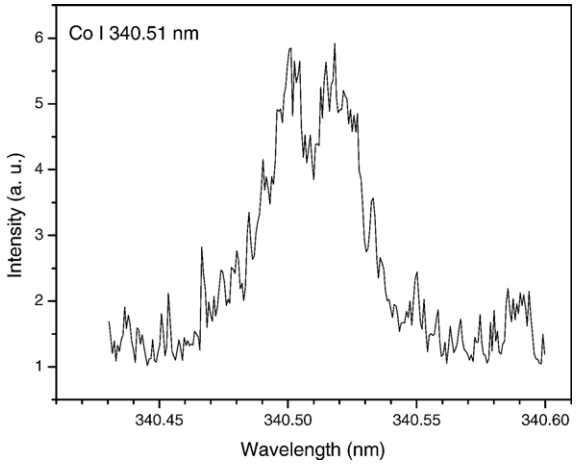

Fig. 2. Line 340.51 nm Co I showing the characteristic dip of a strongly absorbed line from an inhomogeneous plasma.

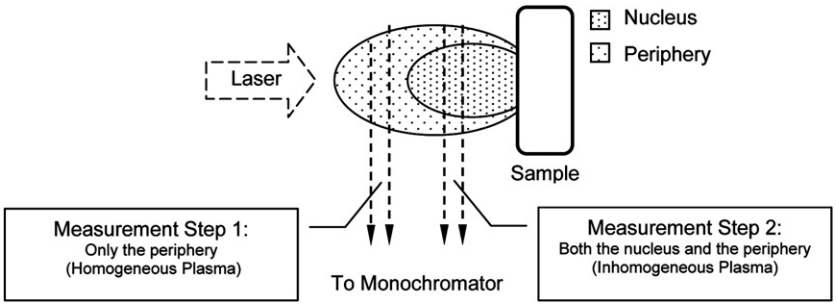

Fig. 3. Factor κ_e of Eq. (3) plotted for several Co I lines as a function of the temperature.

subsequently employed to describe the broadening of the intensity line profiles. Yaroshchyk et al. [19] reported a calibration-free algorithm implemented for the determination of the concentration of the major elements of several samples. The theoretical spectrum, under optically thin and homogeneous plasma conditions, was fitted to the experimental measurements by comparison while varying the temperature and the relative elemental concentrations, allowing a rapid and simultaneous multi-element analysis.

The present work continues the research of LIP characterization. An automatic, moderate time-consuming algorithm has been developed and implemented based on the framework of a two-region plasma, each one in LTE, where self-absorption and inhomogeneity effects are taken into account. The line profiles of three spectral lines of the major component (in our case Co I–II) of a metallic alloy were recorded from both the high-temperature plasma core and the plasma periphery. Thereby, using these spectra and an atomic emission lines database, the plasma parameters (temperature, atom, ion and electron densities) and lines widths that reproduced the experimental line profiles simultaneously were obtained performing a least-squares fitting by means of a self-made computer program.

2. Theoretical

The classical solution to the equation of radiation transfer for the spectral line intensity emitted by an homogeneous plasma is [20]

$$I_\lambda = CU_\lambda(kT)(1 - e^{-\tau_\lambda}), \tag{1}$$

where C is a factor depending on the instrumental set-up, λ (m) is the transition wavelength, U_λ (W m^{-3}) is the distribution for blackbody radiation, kT (eV) is the temperature, and τ_λ (dimensionless) is the optical depth of the plasma. For a plasma in local thermodynamic equilibrium (LTE) the optical depth can be expressed as [12]

$$\tau_\lambda = \kappa_\lambda L = \kappa_e N L g(\lambda). \tag{2}$$

In this expression, κ_e (m^3) is a coefficient that depends on the atomic parameters of the transition and can be calculated if the plasma temperature is known. Namely

$$\kappa_e = \frac{\lambda^4}{8\pi c Q} A_{ji} g_j e^{-\frac{E_i}{kT}}\left(1 - e^{\frac{E_i - E_j}{kT}}\right) \tag{3}$$

where N (m^{-3}) is the density of the emitters in the plasma, L (m) is the absorption path-length and $g(\lambda)$ (m^{-1}) is the normalized line shape. Moreover, Q (dimensionless) is the atomic partition function, A_{ji} (s^{-1}) is the transition probability, g_j (dimensionless) is the statistical weight and E_i and E_j (eV) are the energy levels. The subscripts refer to levels j (upper) and i (lower).

The partition function is

$$Q = \sum_j g_j e^{-\frac{E_j}{kT}}, \tag{4}$$

where the sum is carried out over all the bound levels of the atom or ion. It is computed using energy level data from [21].

In LTE, the ratio of the densities of species with consecutive ionization stages is given by the Saha equation [22],

$$\frac{N_e N^z}{N^{z-1}} = 6.04 \times 10^{21} \frac{Q^z}{Q^{z-1}} kT^{\frac{3}{2}} \exp\left(\frac{-E_\infty^{z-1}}{kT}\right); \tag{5}$$

here, N_e (m^{-3}) is the electron density and E_∞^{z-1} (eV) is the ionization energy of the species $z-1$. The superscript z refers to the ionization degree of the species.

Inhomogeneous plasmas present a spatial distribution of its parameters. Solving a model for these plasmas could be quite cumbersome. The simplest approach is thinking of the plasma as composed of two uniform regions having different densities, temperatures, and optical lengths L_a and L_b along the line of sight. A nucleus (a) with higher temperature, ion and electron

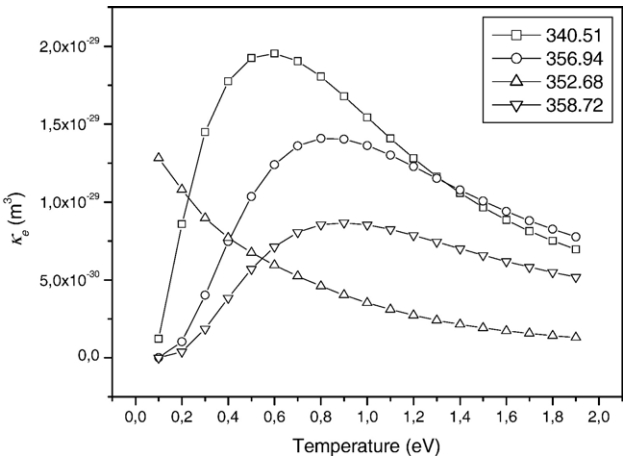

Fig. 4. Two-region plasma model and the measurement procedure.

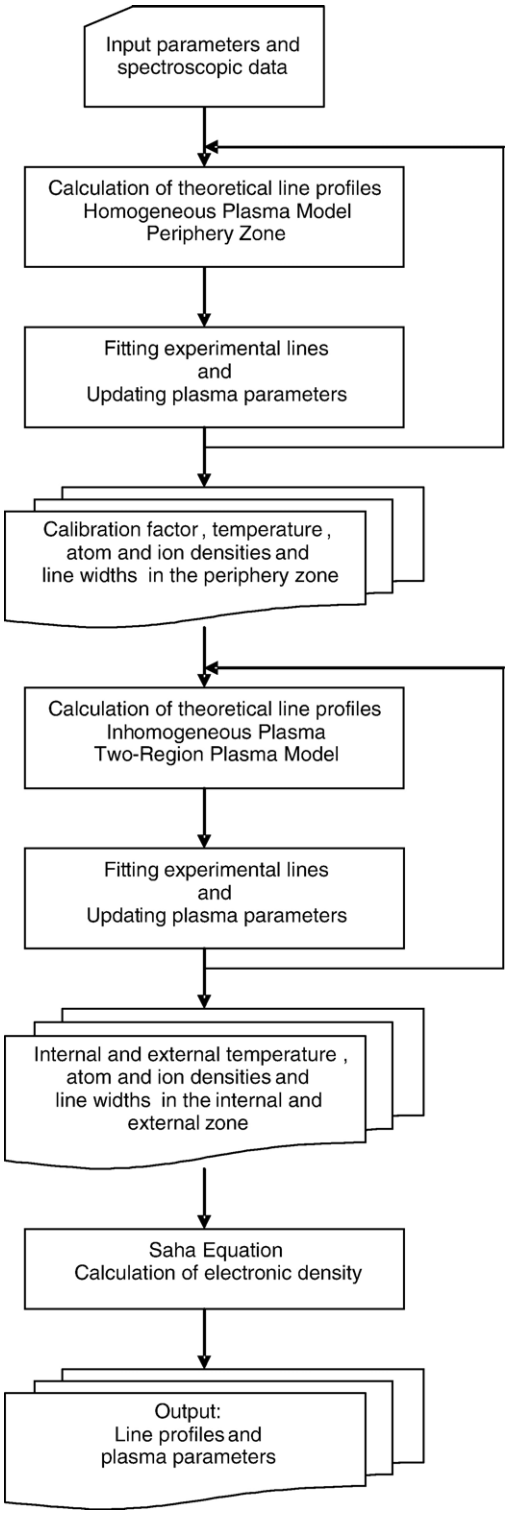

Fig. 5. Schematic diagram of the fitting algorithm used in this work.

densities and a periphery (b) with lower temperature and densities. The values of the plasma parameters inside these regions are assumed to be the averaged values of the real spatial distributions. Hence, the line intensity is given by [19]

$$I_\lambda = CU_\lambda^a(kT_a)(1-e^{-\kappa_\lambda^a L_a})e^{-\kappa_\lambda^a L_b} + CU_\lambda^b(kT_b)(1-e^{-\kappa_\lambda^a L_b}). \quad (6)$$

In this expression, the contributions to the total emission of the two regions can be distinguished: the first term gives the emission from the plasma nucleus absorbed by the plasma periphery, and the second term gives the emission from the plasma periphery alone.

3. Experimental

The experimental set-up was similar to that used in a previous work [23]. It consist of a good spectral resolution

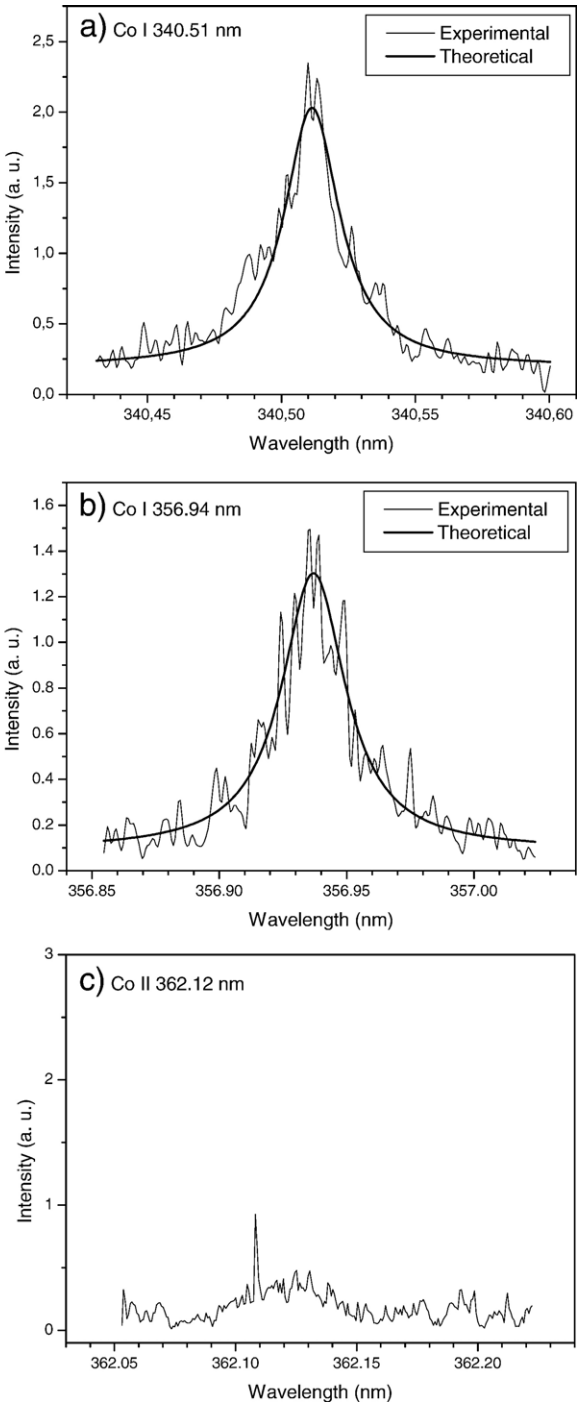

Fig. 6. Co I–II spectral lines recorded in the plasma periphery.

system based on a photomultiplier tube, shown in Fig. 1 and described in detail on Table 1. The target was a ternary alloy Co–Cr–Mo with nominal concentrations of 63% Co, 30% Cr and 7% Mo, and it was fixed to a rotary holder so that every laser shot hit on a fresh site. The emitted plasma radiation was then collected at right angles to the laser beam direction and focused into the entrance slit (40 μm-wide) of a monochromator (resolution 0.01 nm). The detector was a photomultiplier (PM) whose signal was time resolved and averaged with a Box–Car. The delay time was 1500 ns with a gate width of 30 ns.

The emission line profiles were scanned by moving the diffraction grating of the monochromator by means of a step motor, and each experimental point was obtained averaging three laser shots. In order to get spatially resolved measurements of the plasma, a quartz lens was mounted on a translation stage allowing the collection of light from different regions of the plasma along the direction of plume expansion, by moving the plasma image formed on the entrance slit of the monochromator. In such a way, the emission of the plasma from its brightest region (nucleus) and the external edge far away from the sample surface (periphery) were recorded. The measured Co lines and their spectroscopic data are listed in Table 2, according to Ref. [21].

4. Results and discussion

4.1. The model

The goal of this work is to perform a procedure to achieve analytical results from the experimental profiles of selected spectral lines corresponding to specific atomic transitions of Co including the most absorbed spectral lines, which are the easiest to detect.

In a previous work [24], spectral measurements from a plasma zone far away from the sample surface were performed. In order to characterize the plasma, the experimental profiles of eight selected Co and Cr lines (including two resonant lines) were accurately reproduced within an homogeneous framework. In Fig. 2, a typical spectrum of a strongly absorbed self-reversed line from an inhomogeneous plasma experimentally

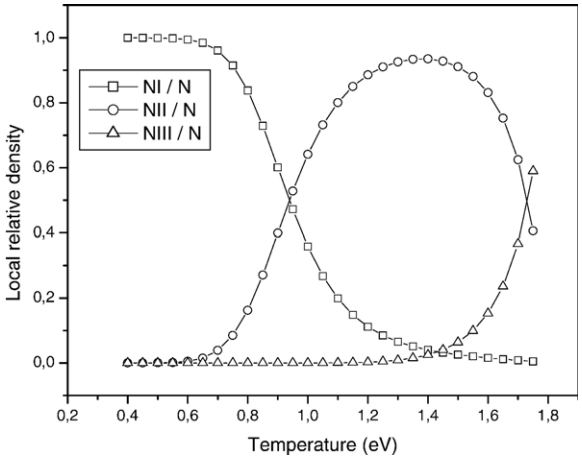

Fig. 7. Relative local populations of the Co species in a LIP, calculated for an electron density of 10^{18} cm^{-3}.

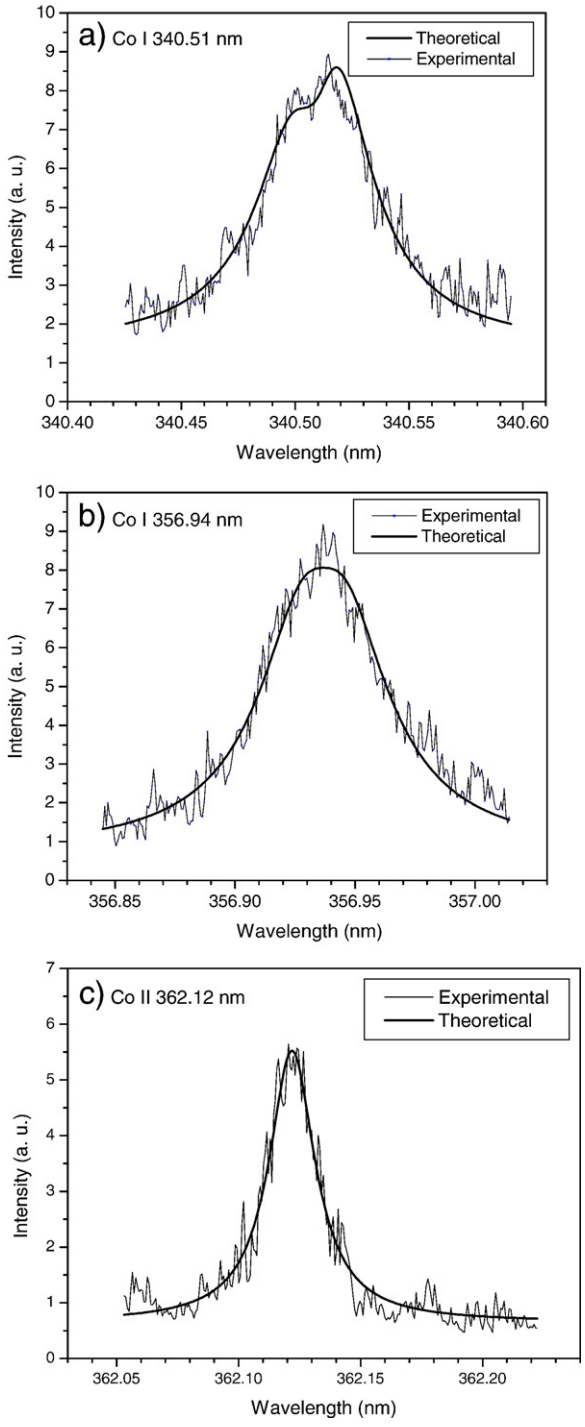

Fig. 8. Co I–II spectral lines recorded in the plasma nucleus.

measured in our experiment can be observed. Thus, in a more realistic approach, a LIP with a nonuniform temperature should be considered. We then assumed that the spectral lines originate in an inhomogeneous plasma consisting in two different regions: a high-temperature dense nucleus surrounded by a colder periphery.

The κ_e factor of Eq. (3) is useful to predict the expected optical depth for different spectral lines and to know in advance which one will result in greater or minor absorption in a LIBS experiment. In Fig. 3, the factor is plotted for several Co I

Table 3
Values of the line parameters of Co obtained by the fitting procedure

Lines (nm)	Width (nm)	
	Nucleus	Periphery
Co I 340.51	0.028±0.001	0.024±0.001
Co I 356.97	0.042±0.001	0.030±0.001
Co II 362.12	0.023±0.001	Not calculated

transitions as a function of the temperature. We can predict that for the typical plasma temperatures obtained in LIP experiences (~1 eV) the lines 340.51 nm and 356.94 nm will be the most absorbed. Therefore, they were selected as the analytical lines together with the line 362.12 of Co II, to verify the ionization equilibrium. Emission spectra were systematically recorded, first from the plasma periphery and, afterwards, from the plasma nucleus under the same experimental conditions (see Fig. 4). Hence, the parameters characterizing both plasma regions were obtained. Despite the fact that the resulting LIP was optically thick and inhomogeneous, it was nevertheless useful to make the Boltzmann plot to get an estimation of the working range of temperatures [25]. Nevertheless, the use of self-absorbed lines from and inhomogeneous plasma in constructing a Boltzmann plot led to a moderate error in the estimation of kT, it originated a significant error in the later determination of electron density. In fact, if conditions of LTE and thin optical thickness are fulfilled in the plasma, the Saha–Boltzmann equation [26] can be used to calculate n_e (cm^{-3}). Namely,

$$n_e = 6.04 \times 10^{21} \frac{I_{\mathrm{Co\ I}}}{I_{\mathrm{Co\ II}}} \frac{\lambda_{\mathrm{Co\ I}}}{\lambda_{\mathrm{Co\ II}}} \frac{A_{ji}^{\mathrm{Co\ II}} g_j^{\mathrm{Co\ II}}}{A_{ji}^{\mathrm{Co\ I}} g_j^{\mathrm{Co\ I}}} e^{\left(\frac{E_{j,\mathrm{Co\ I}} - E_{j,\mathrm{Co\ II}}}{kT}\right)}, \quad (7)$$

where $I_{\mathrm{Co\ I}}$ and $I_{\mathrm{Co\ II}}$ are the integrated intensities of the lines.

On the other hand, we obtained an averaged electron density estimated by measuring the Stark widths of the same lines [26],

$$w \propto \frac{n_e}{(kT)^{1/2}}. \quad (8)$$

The values of n_e obtained with Eqs. (1) and (2) must be of the same order of magnitude if the temperature calculated by means of the Boltzmann plot was approximately correct. But, we observed that both values were in strong discrepancy [27]. Thus, we can conclude that the resulting error in calculating n_e considering the lines as optically thin is considerable and it introduces significant errors in a further analytical determination of the sample composition. This can be overcome by comparing computed line profiles with experimental measurements, as described in the next section.

4.2. The algorithm

The algorithm consists in a self-made computer program, based on systematically computing the profiles of the lines in order to reproduce the measurements performed in both the nucleus and the periphery of the LIP. A schematic diagram of the algorithm is shown in Fig. 5. Once the spectroscopic data of the lines were loaded, as a first step a subroutine was implemented that searched for the values of the parameters that reproduced the profiles of the lines recorded from the plasma periphery. The input parameters of this subroutine were the range of values of the plasma temperature kT_b (0.5–1.5 eV), the calibration factor C, the line widths w_b, and the product $(NL)_b$ of the atom density times the length of the plasma. The temperature was estimated from a Boltzmann plot previously performed assuming, as a rough estimate, an optically thin plasma. A nearly homogeneous emission from this region was expected, hence Eq. (1) was employed to compute the profiles of the lines, being the initial set of parameters updated after each loop. The calculation continued until the set of parameters that provided the best least-squares fitting of the lines was found. Once the measured line profiles of the plasma periphery were accurately reproduced, the next step was carried out by another subroutine. The line profiles were computed for different conditions in order to match the measured line profiles from the plasma nucleus. Now, Eq. (6) describing an inhomogeneous two-zone plasma was employed. The input parameters were the range of values of the temperature kT_a, the line widths w_a, and the products $(NL)_a$ and $(NL)_b$. The latter was recalculated since the optical path changed. The set of parameters previously calculated were also included (i.e.: C, kT_b and w_b). Finally, the electron densities in both regions were obtained using the Saha Eq. (5). The output of the algorithm yielded the plasma parameters and the line widths that reproduced the experimental profiles of the three lines simultaneously.

4.3. Analysis of the emission profiles

Fig. 6a–b show the measured emission spectra of the lines Co I 340.51 nm and Co I 356.94 nm in the plasma periphery together with the theoretical profiles. The line Co II 362.12 nm was also measured in this region, but, as can be seen in Fig. 6c, it is very weak and fades away in the continuum. Thus, the Co II density was assumed negligible within this region in our experimental conditions. Considering that the approximated total density of the Co species in the plasma was $N=N_{\mathrm{I}}+N_{\mathrm{II}}+N_{\mathrm{III}}$, these assumptions were supported using the Saha Eq. (5). Moreover, ionization stages higher than one were not considered. These assumptions were supported using the Saha Eq. (5) to calculate the relative local contributions of the species to the total plasma population for a typical LIP electron density of 10^{18} cm^{-3}, in a similar way as described in [14]. As shown in Fig. 7, for temperatures of about 1 eV the density of the first ion (~64%) is larger than the atom density (~36%) and the density of the second ion is very small (<0.01%). On the other hand, for temperatures of about 0.5 eV the ion density is negligible and the

Table 4
Values of the plasma parameters obtained by the fitting procedure

Parameter	Nucleus	Periphery
kT (eV)	1.08±0.05	0.55±0.05
$NL_{\mathrm{Co\ I}}$ (m^{-2})	$(3.3\pm0.1)\times10^{17}$	$(8.0\pm0.1)\times10^{17}$ (periphery fitting)
		$(3.9\pm0.1)\times10^{18}$ (two-region fitting)
$NL_{\mathrm{Co\ II}}$ (m^{-2})	$(6.90\pm0.01)\times10^{18}$	Not calculated
N_e (cm^{-3})	$\sim1\times10^{17}$	Not calculated

atom density (~99.9%) is the only contribution to the total population. The computed profiles reproduce very well the Co I experimental profiles, showing a Lorentzian shape corresponding to Stark broadening caused by the interactions with plasma electrons, which is the dominant contribution to the line width in LIBS experiments [12]. In Fig. 8, the experimental and theoretical intensity profiles from the plasma nucleus of the lines Co I 340.51 nm, Co I 356.94 and Co II 362.12 nm are shown. The picture of a two-region plasma fit well with the observations, specially the line Co I 340,5 nm which results self-reversed. The resulting plasma parameters: the temperature of both the plasma nucleus and the periphery, the products $(NL)_a$ and $(NL)_b$, and the line widths are shown in Tables 3 and 4. It reveal that the nucleus is populated mainly by Co II at the expense of Co I which is found in the plasma periphery. The ion and electron densities could be calculated only in the nucleus, not in the periphery. Furthermore, larger line widths were obtained in the nucleus than in the periphery, as expected.

5. Conclusions

The aim of the present work is the investigation of standard-less laser-induced plasma characterization employing the strongest lines of the spectra which result the more absorbed in LIBS experiences. A model of a two-region plasma, each one in LTE, where self-absorption effect as well as plasma inhomogeneity are taken into account, was implemented to characterize the physical state of a laser-induced plasma produced on a ternary alloy Co–Cr–Mo. The major component (Co) of the sample was selected as the analyte and the line profiles of three Co I–II lines were recorded with good resolution and fitted by means of a self-made least-squares computer algorithm that calculated the plasma and line parameters of both the plasma nucleus and the periphery, that accurately reproduced the experimental line profiles. The algorithm is moderately time-consuming depending on the initial range of the parameter values and was implemented only with three spectral lines. In fact, more lines can be included as well as code improvements are provided. The obtained results demonstrated that the picture of a two-region plasma fit well with the observations and allowed the estimation of atom, ion and electron densities in a laser-induced plasma in air at atmospheric pressure. The plasma characterization provided valuable insight for a future analytical procedure.

Acknowledgements

This work has been supported by the project PIP6473 of CONICET, Argentina. The authors gratefully acknowledge Dr H. F. Ranea Sandoval for his valuable suggestions about this work.

References

[1] E. Tognoni, V. Palleschi, M. Corsi, G. Cristoforetti, Quantitative microanalysis by laser-induced breakdown spectroscopy: a review of the experimental approaches, Spectrochim. Acta Part B 57 (2002) 1115–1130.
[2] A. Aragón, J. Bengoechea, J.A. Aguilera, Asymmetric Stark broadening of the Fe I 538.34 nm emission line in a laser induced plasma, Spectrochim. Acta Part B 60 (2005) 897–904.
[3] J. Bengoechea, J.A. Aguilera, C. Aragón, Application of laser-induced plasma spectroscopy to the measurement of Stark broadening parameters, Spectrochim. Acta Part B 61 (2006) 69–80.
[4] C. Colón, A. Alonso-Medina, Application of a laser produced plasma: experimental Stark widths of single ionized lead lines, Spectrochim. Acta Part B 61 (2006) 856–863.
[5] O.E.M. Pohler, Failures of metallic orthopedic implants, metals handbook, American Society for Metals, 9th ed. Failure Analysis and Prevention, vol. 11,, ASM, Metals Park, OH, 1986, p. 670.
[6] M. Sabsabi, P. Cielo, Quantitative analysis of aluminum alloys by laser-induced breakdown spectroscopy and plasma characterization, Appl. Spectrosc. 49 (1995) 499–507.
[7] D.E. Kim, K.J. Yoo, H.K. Park, K.J. Oh, D.W. Kim, Quantitative analysis of aluminum impurities in zinc alloy by laser-induced breakdown spectroscopy, Appl. Spectrosc. 51 (22) (1997) 22–29.
[8] C. Aragón, J.A. Aguilera, F. Peñalba, Improvements in quantitative analysis of steel composition by laser-induced breakdown spectroscopy at atmospheric pressure using an infrared Nd:YAG laser, Appl. Spectrosc. 53 (1999) 1259–1267.
[9] M. Kuzuya, H. Aranami, Analysis of a high-concentration copper in metal alloys by emission spectroscopy of a laser-produced plasma in air at atmospheric pressure, Spectrochim. Acta Part B 55 (2000) 1423–1430.
[10] J.M. Gomba, C. D'Angelo, D. Bertuccelli, G. Bertuccelli, Spectroscopic characterization of laser induced breakdown in aluminum–lithium alloy samples for quantitative determination of traces, Spectrochim. Acta Part B 56 (2001) 695–705.
[11] G. Tondello, E. Jannitti, A.M. Malvezzi, Line broadening and self-absorption of Be IV in a laser-produced plasma, Phys. Rev., A 16 (4) (1977) 1705–1714.
[12] C. Aragón, J. Bengoechea, J.A. Aguilera, Influence of the optical depth on spectral line emission from laser-induced plasmas, Spectrochim. Acta Part B 56 (2001) 619–628.
[13] J.A. Aguilera, J. Bengoechea, C. Aragón, Spatial characterization of laser induced plasmas obtained in air and argon with different laser focusing distances, Spectrochim. Acta Part B 59 (2004) 461–469.
[14] J.A. Aguilera, C. Aragón, Characterization of a laser-induced plasma by spatially resolved spectroscopy of neutral atom and ion emissions. Comparison of local and spatially integrated measurements, Spectrochim. Acta Part B 59 (2004) 1861–1876.
[15] L.J. Radziemski, D.A. Cremers, Laser-Induced Plasmas and Applications, Marcel Dekker Inc., New York, 1989.
[16] J. Hermann, C. Boulmer-Leborgne, D. Hong, Diagnostic of the early phase of an ultraviolet laser induced plasma by spectral line analysis considering self-absorption, J. Appl. Phys. 83 (2) (1998) 691–696.
[17] D. Bulajic, M. Corsi, G. Cristoforetti, S. Legnaioli, V. Palleschi, A. Salvetti, E. Tognoni, A procedure for correcting self-absorption in calibration free-laser induced breakdown spectroscopy, Spectrochim. Acta Part B 57 (2002) 339–353.
[18] J.A. Aguilera, J. Bengoechea, C. Aragón, Curves of growth of spectral lines emitted by a laser-induced plasma: influence of the temporal evolution and spatial inhomogeneity of the plasma, Spectrochim. Acta Part B 58 (2002) 221–237.
[19] P. Yaroshchyk, D. Body, R. Morrison, B. Chadwick, A semi-quantitative standard-less analysis method for laser-induced breakdown spectroscopy, Spectrochim. Acta Part B 61 (2006) 200–209.
[20] Corney, Atomic and Laser Spectroscopy, Oxford University Press, Great Britain, 1979.
[21] NIST electronic database, at http://physics.nist.gov/PhysRefData.
[22] J. Ritcher, Radiation of hot gases, in: W. Lotche-Holtgreven (Ed.), Plasma Diagnostics, John Wiley & Sons Inc., Amsterdam, 1968, pp. 9–20.
[23] D.M. Díaz Pace, C.A. D'Angelo, D. Bertuccelli, G. Bertuccelli, Analysis of heavy metals in liquids using laser induced breakdown spectroscopy by liquid-to-solid matrix conversion, Spectrochim. Acta Part B 61 (2006) 929–933.
[24] C. D'Angelo, D. Díaz Pace, D. Bertuccelli, G. Bertuccelli, Spectroscopic analysis of signals from LIBS experiments, in: A. Marcano, J.L. Paz

(Eds.), 5th Iberoamerican Meeting on Optics and 8th Latin American Meeting on Optics, Lasers, and their Applications, SPIE Proceedings, vol. 5622, 2004, pp. 1037–1042.
[25] C. D'Angelo, D. Díaz Pace, D. Bertuccelli, G. Bertuccelli, Spectroscopic analysis of signals on LIBS experiences. Fit of experimental measurements, in: A. Marcano, J.L. Paz (Eds.), 5th Iberoamerican Meeting on Optics and 8th Latin American Meeting on Optics, Lasers, and their Applications. SPIE Proceedings, vol. 5622, 2004, pp. 1055–1060.
[26] H.R. Griem, Plasma Spectroscopy, Mc Graw-Hill, New York, 1964.
[27] C.A. D'Angelo, Estudio de plasmas formados sobre aleaciones metálicas mediante la técnica LIBS, Tesis de Doctorado, Fac. de Ciencias Exactas, UNCPBA, Tandil (2006).